Numerical Control of a Two-dimensional Channel Flow with Porous Expanding Walls at Different Temperatures

Elkana Pemha[1], Jacques Hona[1,*] and Elisabeth Ngo Nyobe[2]
[1]Applied Mechanics Laboratory, Faculty of Science, University of Yaoundé I, P.O. Box 7389 Yaoundé, Cameroon, E-mail address: elkanaderbeau@yahoo.fr
[2]Department of Mathematics and Physical Science, National Advanced School of Engineering, University of Yaoundé I, P.O. Box 8390 Yaoundé, Cameroon, E-mail address: nyobe _eli@yahoo.fr

Received date: 4 September 2014; Accepted date: 20 February 2015

ABSTRACT

The laminar incompressible flow develops within a channel with two permeable walls which undergo expansion. The flow is injected through the two uniformly porous walls kept at different temperatures. The mathematical model of the problem is obtained by applying mass, momentum and energy conservations. Using the similarity transformation technique, the governing equations give rise to two nonlinear ordinary differential equations. The numerical procedure for solving the differential equations of the problem is detailed. The numerical results are analyzed and the influences of the Reynolds number, the Prandtl number, and the wall moving ratio are discussed. The variations of the velocity distribution, thermal gradients, and pressure gradients are obtained. In particular, when low injection occurs concurrently with high expansion, the reverse flow takes place inside the channel. High injection provides oscillatory pressure gradients under different expansion ratios.

Keywords: two-dimensional flows; heat transfer; porous expanding walls; Navier-Stokes equations; similarity solutions; numerical shooting technique

1. INTRODUCTION

The incompressible fluid flows between two permeable walls are widely studied in the literature [1–9] due to their several direct applications. These applications include filtration, membrane separation processes, biological transport processes, solar energy collectors, and also the control of some industrial flow processes with injection or suction.

In particular, the moving wall channel with injection is used to model the slab rocket motors in order to enhance their performances and to perform the hybrid motors. Furthermore, the injection-driven flow through porous channels with orthogonally moving walls has gained great importance because of its applications in pulsating diaphragms regarding biophysical flows. The applications of the present study also include filtration and purification in the biopharmaceutical industry. Since the theory is an indispensable support to ensure a deeper understanding of some practical processes, the present numerical investigation is devoted to extend the solution range to physical settings.

The work of Berman [10] about a laminar flow through a rectangular permeable channel has inspired many later studies [11–15]. In this pioneer study of Berman [10], the steady flow is controlled by means of the Reynolds number defined on the base of the channel half-spacing and the injection velocity. The study of flows in porous rectangular channels, named Berman flows by some authors, is also extended in the case of channels with a cylindrical configuration [16–19].

In most of the studies of Berman flow in above references where the similarity method is used; the modeling process leads to solving a fourth-order nonlinear ordinary differential equation by means of a numerical integration. In fact, seeking solutions by numerical integration is a powerful theoretical

*Corresponding Author: Tel.: +237 691 36 44 75, E-mail address: honajacques@yahoo.fr

technique that many scientists [11, 15, 18, 20] are making increasing use for the investigation of fluid flows in various configurations.

When thermal effects are taking into consideration through the channel, the flow is governed by the Navier-Stokes equations and the energy equation [5, 6, 8, 21]. These differential equations are in partial coupling [19] if the difference of temperatures between the walls is not high enough to produce significant changes in the physical properties of the fluid. However, the differential equations which describe the flow inside the channel are fully coupled if some physical properties of the fluid vary [21].

The present study describes the similarity solutions for the steady flow through a uniformly porous channel with orthogonally moving walls which are fixed at different temperatures. The novelty is the investigation of wall expansion which occurs concurrently with injection and heat transfer inside a rectangular channel. The problem is defined between two outer walls and an open inner wall located at the midsection plane of the channel. More precisely, the flow is modeled in two half domains, since the channel consists of two rigid porous surfaces representing the cold and the hot walls and a symmetry plane which divides the flow domain into two identical parts. Our desire is to investigate the effects of simultaneous injection and expansion processes at walls on the laminar flow inside the symmetric channel.

We shall formulate in Section 2 the mathematical model of the problem. Section 3 is devoted to the similarity transformation of the governing equations. In Section 4, the numerical integration is detailed, while the results discussion is performed in Section 5 in order to provide the physical significance of solutions of the problem under study. Section 6 is reserved to the conclusions.

2. GOVERNING EQUATIONS

Incompressible viscous fluid is uniformly injected through a rectangular porous channel which has walls at $y = -b$ and $y = +b$ as shown in Figure 1. Both walls are distanced by $2b$ known as the channel width, while h denotes the height of the channel such that $h > b$. The length of the channel along the streamwise direction has an infinite end, and a head-end at $x = 0$ is closed by an impermeable membrane which allows the channel expansion with a uniform velocity defined as $\dot{b} = db/dt$. The flow is assumed to be two-dimensional, so the velocity field has components as $(V_x, V_y, 0)$, where V_x is the streamwise velocity, and V_y denotes the transverse or the normal velocity. By taking into account the existence of a symmetry plane in the middle of the flow region, the flow is defined in two half domains of the channel. T_0 denotes the fixed temperature of the hot wall at $y = +b$, and $T_{\min} = 0$ is the fixed temperature of the cold wall at $y = -b$. The temperature of the fluid is represented by T, and p is the pressure. The constant physical properties of the fluid are the specific mass ρ, the thermal conductivity κ, and the kinematic viscosity ν.

In the absence of body forces, considering a plane Cartesian coordinate system (x, y), the equations describing the flow and the heat transfer inside the channel are written in terms of above dimensional variables using mass, momentum and energy conservations

$$\frac{\partial V_x}{\partial x} + \frac{\partial V_y}{\partial y} = 0 \tag{1}$$

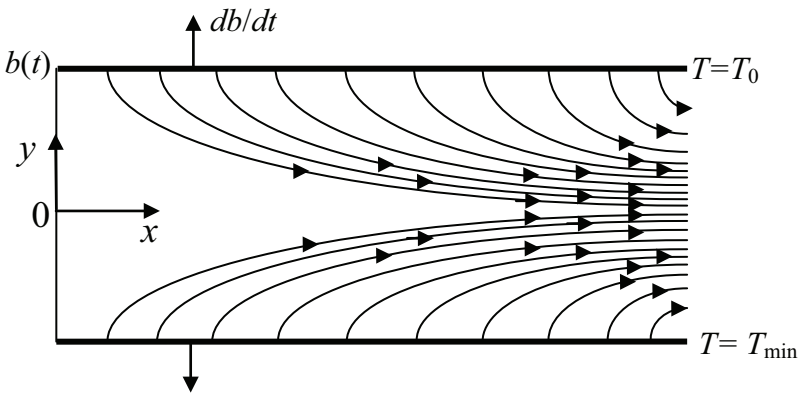

Figure 1. Geometry of the channel with typical stream lines representing the flow pattern of a symmetric similarity solution for the injection problem.

$$\frac{\partial V_x}{\partial t}+V_x\frac{\partial V_x}{\partial x}+V_y\frac{\partial V_x}{\partial y}=-\frac{1}{\rho}\frac{\partial p}{\partial x}+\nu\left(\frac{\partial^2 V_x}{\partial x^2}+\frac{\partial^2 V_x}{\partial y^2}\right) \tag{2}$$

$$\frac{\partial V_y}{\partial t}+V_x\frac{\partial V_y}{\partial x}+V_y\frac{\partial V_y}{\partial y}=-\frac{1}{\rho}\frac{\partial p}{\partial y}+\nu\left(\frac{\partial^2 V_y}{\partial x^2}+\frac{\partial^2 V_y}{\partial y^2}\right) \tag{3}$$

$$\frac{\partial T}{\partial t}+V_x\frac{\partial T}{\partial x}+V_y\frac{\partial T}{\partial y}=\frac{\kappa}{\rho}\left(\frac{\partial^2 T}{\partial x^2}+\frac{\partial^2 T}{\partial y^2}\right) \tag{4}$$

Equation (1) is the continuity equation, while (2) and (3) are the Navier-Stokes equations and (4) is the energy equation. The boundary conditions are

$$\begin{array}{llll} V_x=0, & V_y=V, & T=0 & \text{at} \quad y=-b(t) \\ \dfrac{\partial V_x}{\partial y}=0, & V_y=0, & \dfrac{\partial T}{\partial y}=\dfrac{T_0}{2b} & \text{at} \quad y=0 \\ V_x=0, & V_y=-V, & T=T_0 & \text{at} \quad y=b(t) \end{array} \tag{5}$$

In addition, there is no fluid motion at the closed end ($x = 0$), such that $V_x = 0$, $V_y = 0$ at $x = 0$, that is the no-slip condition. Furthermore, the influence of the infinite end along the streamwise direction is neglected as the channel length is great compared to its width. The absolute velocity V through the boundary conditions depends on the relative injection speed V_0, and the wall moving velocity $\dot{b}$ also known as the entrainment velocity of fluid particles:

$$V = V_0 - \dot{b} \tag{6}$$

In Equation (6), V is assumed to be independent of position, and $\dot{b}$ is constant, so the relative injection velocity V_0 is spatially uniform.

The volume ϑ of fluid extending from the close membrane (at $x = 0$) to an arbitrary location x is given by:

$$\vartheta = 2bhx \tag{7}$$

while the resulting porous surface A of the two horizontal rigid walls is

$$A = 2hx \tag{8}$$

and the cross section surface S of the channel, perpendicular to the streamwise direction is defined as:

$$S = 2bh \tag{9}$$

At this stage, it is opportune to define the mean flow velocity U at the arbitrary end x, averaged over the cross section by the following integral form:

$$U = \frac{1}{S}\int_{(S)} V_x(x, y, t)\,dS \tag{10}$$

Our aim is to establish the fundamental relation of mass conservation relative to the channel with the assumption that the mass withdrawal phenomenon occurs per unit time through the arbitrary end cross section, while the mass addition scenario is observed at porous walls due to injection. Then, the variation of mass per unit time in the channel's volume is obtained:

$$\frac{\partial}{\partial t}\int_{(\vartheta)} \rho\, d\vartheta = \rho A V_0 - \int_{(S)} \rho V_x dS \tag{11}$$

where $d\vartheta = d(Sx)$ and $dS = d(2bh)$. By introducing the formula (10) in Equation (11), the mass conservation becomes:

$$\rho x\frac{\partial S}{\partial t} = \rho A V_0 - \rho S U \tag{12}$$

The strategy consists to obtain an expression of the mean velocity U as function of the absolute velocity V, because this expression will help for the non-dimensional formulation of the problem

which follows in Section 3. By taking into account the formulas (6), (7) and (8), it appears from Equation (12) that:

$$U = \frac{A}{S}V_0 - \frac{x}{S}\frac{\partial S}{\partial t} = \frac{x}{b}\left(V_0 - \dot{b}\right) = \frac{x}{b}V \tag{13}$$

Equation (13) shows that U and V are proportional; such a behavior leads to understand that, the high injection speed at walls increases the mean velocity at the arbitrary end in the streamwise direction in order to ensure mass conservation through the channel. In addition, high expansion diminishes the mean flow velocity.

As the velocity field has two components according to the two-dimensional configuration of the problem, it is often convenient to introduce the stream function in the governing equations in order to substitute the streamwise and the transverse velocity components by a single function ψ, as follows:

$$V_x = \frac{\partial \psi}{\partial y} \quad \text{and} \quad V_y = -\frac{\partial \psi}{\partial x} \tag{14}$$

At this stage, by taking the curl of the momentum equation, the vorticity transport equation is produced and is satisfied by the stream function ψ. Due to the introduction of the stream function, the governing equations become:

$$\frac{\partial}{\partial t}\Delta\psi + \frac{\partial \psi}{\partial y}\frac{\partial}{\partial x}\Delta\psi - \frac{\partial \psi}{\partial x}\frac{\partial}{\partial y}\Delta\psi = \nu\Delta^2\psi \tag{15}$$

$$\frac{\partial T}{\partial t} + \frac{\partial \psi}{\partial y}\frac{\partial T}{\partial x} - \frac{\partial \psi}{\partial x}\frac{\partial T}{\partial y} = \frac{\kappa}{\rho}\Delta T \tag{16}$$

where $\Delta = \frac{\partial^2}{\partial x^2} + \frac{\partial^2}{\partial y^2}$. The boundary conditions associated with Equations (15) and (16) are deduced as follows:

$$\begin{aligned}
&\frac{\partial \psi}{\partial y} = 0, \quad \frac{\partial \psi}{\partial x} = -V, \quad T = 0 \quad \text{at} \quad y = -b(t) \\
&\frac{\partial^2 \psi}{\partial y^2} = 0, \quad \frac{\partial \psi}{\partial x} = 0, \quad \frac{\partial T}{\partial y} = \frac{T_0}{2b} \quad \text{at} \quad y = 0 \\
&\frac{\partial \psi}{\partial y} = 0, \quad \frac{\partial \psi}{\partial x} = V, \quad T = T_0 \quad \text{at} \quad y = b(t)
\end{aligned} \tag{17}$$

3. SIMILARITY FORMULATION

The nondimensional formulation is used to produce some control parameters of the problem by taking into consideration the boundary conditions and the geometry of the channel. Let us consider functions Φ and Θ as the nondimensional stream function and the nondimensional temperature, respectively. These nondimensional functions are related to the dimensional stream function ψ and temperature T by the following formulas:

$$\begin{aligned}
&\psi(x,y,t) = \frac{\nu x}{b}\Phi(\eta,t) \\
&T(x,y,t) = T_0\,\Theta(\eta,t) \\
&\eta = \frac{y}{b(t)}
\end{aligned} \tag{18}$$

where η is the dimensionless similarity variable independent of the streamwise coordinate. The similarity properties of Equations (18) are in accordance with a Berman type similarity form in which

the length of the channel along the streamwise direction x is considered as a constant. By introducing expressions (18) in Equations (15) and (16), the nondimensional functions Φ and Θ satisfy the following set of partial differential equations:

$$\frac{b^2}{\nu}\frac{\partial}{\partial t}\left(\frac{\partial^2\Phi}{\partial\eta^2}\right)+\frac{\partial\Phi}{\partial\eta}\frac{\partial^2\Phi}{\partial\eta^2}-\Phi\frac{\partial^3\Phi}{\partial\eta^3}-\beta\eta\frac{\partial^3\Phi}{\partial\eta^3}-3\beta\frac{\partial^2\Phi}{\partial\eta^2}=\frac{\partial^4\Phi}{\partial\eta^4} \tag{19}$$

$$\frac{b^2}{\nu}\frac{\partial\Theta}{\partial t}-\Phi\frac{\partial\Theta}{\partial\eta}-\beta\eta\frac{\partial\Theta}{\partial\eta}=\frac{1}{\mathrm{Pr}}\frac{\partial^2\Theta}{\partial\eta^2} \tag{20}$$

where the Prandtl number $\mathrm{Pr} = \rho\nu/\kappa$ and the expansion ratio $\beta = b\dot{b}/\nu$ are derived. The corresponding boundary conditions are given:

$$\begin{aligned}
&\frac{\partial\Phi}{\partial\eta}=0, && \Phi=-R, && \Theta=0 && \text{at}\quad \eta=-1\\
&\frac{\partial^2\Phi}{\partial\eta^2}=0, && \Phi=0, && \frac{\partial\Theta}{\partial\eta}=0.5 && \text{at}\quad \eta=0\\
&\frac{\partial\Phi}{\partial\eta}=0, && \Phi=R, && \Theta=1 && \text{at}\quad \eta=1
\end{aligned} \tag{21}$$

where $R = Vb/\nu$ denotes the Reynolds number. Equations (19) and (20) with the boundary conditions (21) describe the unsteady flow. In order to solve these partial differential equations, an initial condition is required, but our attention is focused only on the steady flow, because the unsteady flow which gives rise to the time-dependent solutions does not influence the dynamics discussed in this work. Furthermore, the unique significant attention with the unsteady flow is when the desire is to find oscillatory solutions by using the time as parameter.

However, steady solutions are found by expressing functions Φ and Θ as

$$\begin{aligned}
\Phi(\eta, t) &= \varphi(\eta)\\
\Theta(\eta, t) &= \theta(\eta)
\end{aligned} \tag{22}$$

Normalizing the streamwise velocity by its mean value U over the cross section of the channel, and the normal velocity by its value at the rigid porous wall $(-V)$ in accordance with the boundary conditions (5), expressions of the nondimensional velocity components V_x^* and V_y^* are obtained as follows:

$$V_x^* = V_x/U = \varphi^{(1)}/R\,, \qquad V_y^* = V_y/(-V) = \varphi/R \tag{23}$$

By considering the flow properties of Equations (22), the problem is reduced to ordinary differential equations and boundary conditions as follows:

$$\begin{aligned}
&\varphi^{(4)}+\varphi\varphi^{(3)}-\varphi^{(1)}\varphi^{(2)}+\beta\eta\varphi^{(3)}+3\beta\varphi^{(2)}=0\\
&\theta^{(2)}+\mathrm{Pr}\,\varphi\theta^{(1)}+\mathrm{Pr}\,\beta\eta\theta^{(1)}=0\\
&\varphi(-1)=-R, \quad \varphi(0)=0, \quad \varphi(1)=R\\
&\varphi^{(1)}(-1)=0, \quad \varphi^{(2)}(0)=0, \quad \varphi^{(1)}(1)=0\\
&\theta(-1)=0, \quad \theta^{(1)}(0)=0.5, \quad \theta(1)=1
\end{aligned} \tag{24}$$

where $\varphi^{(i)} = d^i\varphi/d\eta^i$ and $\theta^{(i)} = d^i\theta/d\eta^i$.

Nondimensional variables for length and pressure are measured in units of b and $\rho\nu^2/b^2$, respectively; then expressions about the normalized streamwise pressure gradient per unit length $\frac{1}{x^*}\frac{\partial p^*}{\partial x^*}$ and normal pressure gradient $\frac{\partial p^*}{\partial\eta}$ can now be derived knowing the evolution of the stream function. Considering the momentum Equations (2) and (3) by setting φ as function of η only, we obtain:

$$\frac{1}{x^*}\frac{\partial p^*}{\partial x^*} = \varphi^{(3)} + \varphi\varphi^{(2)} + \left(2\beta - \varphi^{(1)}\right)\varphi^{(1)} + \beta\eta\varphi^{(2)} = \text{constant}$$

$$\frac{\partial p^*}{\partial \eta} = p^{(1)*}(\eta) = -\left(\varphi^{(2)} + \varphi\varphi^{(1)} + \beta(\varphi + \eta\varphi^{(1)})\right) \tag{25}$$

It follows that the nondimensional streamwise pressure gradient per unit length is constant through the channel since it is equivalent to the integral of the left hand side of the similarity vorticity equation.

4. NUMERICAL INTEGRATION

The integration is performed in two stages. The first stage consists to find the partial solution of Equations (24) in the interval $-1 \le \eta \le 0$ as a nonlinear two-point boundary-value problem using the numerical shooting method, associated with the rapidly converging fourth-order Runge-Kutta algorithm. About the second stage, we use the same numerical scheme by applying the boundary conditions relative to the interval $0 \le \eta \le 1$ for obtaining the complete solution. In this Section, we only describe the first stage of calculations, since the second one is realized by changing the boundary conditions.

To start, we transform the boundary value problem (24) into an initial value one at point $\eta = -1$. Hence, six initial conditions are required, but the problem provides only three conditions at point $\eta = -1$, such that $\varphi(-1) = -R$, $\varphi^{(1)}(-1) = 0$, $\theta(-1) = 0$; then, to well formulate the initial value problem, it is mandatory to add three additional arbitrary conditions ($\varphi^{(2)}(-1) = a_1$, $\varphi^{(3)}(-1) = a_2$, $\theta^{(1)}(-1) = a_3$). To solve the initial value problem applying the fourth-order Runge-Kutta algorithm, we rewrite the ordinary equations of problem (24) as a system of six first-order coupled differential equations by setting: $\varphi_1 = \varphi$, $\varphi_2 = \varphi^{(1)}$, $\varphi_3 = \varphi^{(2)}$, $\varphi_4 = \varphi^{(3)}$, $\theta_1 = \theta$, and $\theta_2 = \theta^{(1)}$. Hence, the six first-order coupled differential equations and the initial conditions are presented as follows:

$$\begin{aligned}
&\theta_1^{(1)} = \theta_2 \\
&\varphi_1^{(1)} = \varphi_2 \\
&\varphi_2^{(1)} = \varphi_3 \\
&\varphi_3^{(1)} = \varphi_4 \\
&\theta_2^{(1)} = -\mathrm{Pr}\varphi_1\theta_2 - \mathrm{Pr}\beta\eta\theta_2 \\
&\varphi_4^{(1)} = \varphi_1\varphi_4 + \varphi_2\varphi_3 - \beta\eta\varphi_4 - 3\beta\varphi_3 \\
&\varphi_1(-1) = -R,\ \varphi_2(-1) = 0,\ \varphi_3(-1) = a_1,\ \varphi_4(-1) = a_2,\ \theta_1(-1) = 0,\ \theta_2(-1) = a_3
\end{aligned} \tag{26}$$

The values of functions φ, θ and those of their derivatives are calculated for any arbitrary three initial guesses a_1, a_2 and a_3, applying the fourth-order Runge-Kutta algorithm. In addition, the three boundary conditions at the midsection plane $\eta = 0$, $\varphi_1(0, a_1, a_2) = \varphi(0, a_1, a_2)$; $\varphi_3(0, a_1, a_2) = \varphi^{(2)}(0, a_1, a_2)$; $\theta_2(0, a_1, a_2, a_3) = \theta^{(1)}(0, a_1, a_2, a_3)$ are also calculated. This means that, the solution of the problem depends on three unspecified start-up conditions a_1, a_2 and a_3.

The best initial guesses a_1^*, a_2^* and a_3^* are the ones for which the boundary conditions of the problem at $\eta = 0$ are satisfied, that is $\varphi(0, a_1, a_2) = 0$, $\varphi^{(2)}(0, a_1, a_2) = 0$, $\theta^{(1)}(0, a_1, a_2, a_3) = 0.5$. The determination of a_1^*, a_2^* and a_3^* leads to an optimization type problem which consists to minimize the following function

$$F(a_1, a_2, a_3) = (\varphi(0, a_1, a_2) - 0)^2 + (\varphi^{(2)}(0, a_1, a_2) - 0)^2 + (\theta^{(1)}(0, a_1, a_2, a_3) - 0.5)^2 \tag{27}$$

The Newton's generalized method is applied for seeking the zeros a_1^*, a_2^*, a_3^* of function F. The algorithm of this method requires updating the initial guesses by the following formula:

$$\begin{bmatrix} a_1 \\ a_2 \\ a_3 \end{bmatrix}_{n+1} = \begin{bmatrix} a_1 \\ a_2 \\ a_3 \end{bmatrix}_n - [J]^{-1} . \begin{bmatrix} \varphi(0,a_1,a_2) - 0 \\ \varphi^{(2)}(0,a_1,a_2) - 0 \\ \theta^{(1)}(0,a_1,a_2,a_3) - 0.5 \end{bmatrix} \tag{28}$$

where n is the iteration index and $[J]^{-1}$ denotes the inverted Jacobian matrix. The Jacobian is defined as follows:

$$J = \begin{bmatrix} \dfrac{\partial G_1}{\partial a_1} & \dfrac{\partial G_1}{\partial a_2} & \dfrac{\partial \mathrm{G}_1}{\partial a_3} \\ \dfrac{\partial G_2}{\partial a_1} & \dfrac{\partial G_2}{\partial a_2} & \dfrac{\partial \mathrm{G}_2}{\partial a_3} \\ \dfrac{\partial G_3}{\partial a_1} & \dfrac{\partial G_3}{\partial a_2} & \dfrac{\partial G_3}{\partial a_3} \end{bmatrix} = \begin{bmatrix} u_1(0) & u_2(0) & u_3(0) \\ u_1^{(2)}(0) & u_2^{(2)}(0) & u_3^{(2)}(0) \\ w_1^{(1)}(0) & w_2^{(1)}(0) & w_3^{(1)}(0) \end{bmatrix} \tag{29}$$

The quantities G_1, G_2 and G_3 are defined by:

$$\begin{aligned} G_1 &= \varphi(0, a_1, a_2) - 0 \\ G_2 &= \varphi^{(2)}(0, a_1, a_2) - 0 \\ G_3 &= \theta^{(1)}(0, a_1, a_2, a_3) - 0.5 \end{aligned} \tag{30}$$

The new functions u_j and w_j, $j = 1, 2, 3$, are defined as:

$$u_j(\eta, a_1, a_2) = \frac{\partial \varphi}{\partial a_j}, \qquad w_j(\eta, a_1, a_2, a_3) = \frac{\partial \theta}{\partial a_j} \tag{31}$$

It appears that the components of the Jacobian matrix are the values of functions u_j, $u_j^{(2)}$ and $w_j^{(1)}$ at $\eta = 0$. In fact, functions u_j and w_j satisfy three sets of coupled differential equations obtained by taking the derivative of the set of Equations (26) with respect to a_j, $j = 1, 2, 3$, knowing that:

$$\begin{aligned} \frac{\partial \varphi^{(i)}}{\partial a_j} &= \frac{\partial}{\partial a_j}\left(\frac{\partial^i \varphi}{\partial \eta^i}\right) = \frac{\partial^i}{\partial \eta^i}\left(\frac{\partial \varphi}{\partial a_j}\right) = u_j^{(i)} \\ \frac{\partial \theta^{(i)}}{\partial a_j} &= \frac{\partial}{\partial a_j}\left(\frac{\partial^i \theta}{\partial \eta^i}\right) = \frac{\partial^i}{\partial \eta^i}\left(\frac{\partial \theta}{\partial a_j}\right) = w_j^{(i)} \end{aligned} \tag{32}$$

In what follows, the solutions are interpreted in terms of velocity components, pressure gradient, temperature and thermal gradients.

5. RESULTS DISCUSSION

The purpose at this stage is to highlight the flow character over different values of control parameters of the problem under study.

Flow reversal occurs through the channel for high expansion in the case of low injection as presented in Figure 2(a). More precisely, flow reversal, also known as backward flow, manifests itself as negative values of the treamwise velocity, while low injection corresponds to small values of the Reynolds number. In other words, low injection speed and high expansion produce the reverse flow in the attempt to satisfy mass conservation inside the channel. The scenario of flow reversal highlighted in Figure 2(a) is that, when fluid particles are injected at walls with low Reynolds number, high expansion tends to produce a mass withdrawal phenomenon also known as suction. Indeed, the mass withdrawal phenomenon is a process for which fluid particles leave the channel for suction motion at walls. Since injection and suction are two opposing processes which could occur through the channel, this leads to conclusion that, some collision zones exist in the flow field under study. These collision zones were found in previous studies [16, 22], but do not interest the dynamics discussed in the present work.

Figure 2(a) shows that the streamwise velocity decreases with the expansion ratio in a large area including the vicinity of both walls, but the increase is observed only around the center of the channel. This behavior highlights the fact that, in Figure 2(a) different behaviors of the streamwise velocity are observed between the rest of the channel and the area situated around the middle of the flow region due to the expansion process. In light of Figure 2(b) and (c), flow reversal disappears with the increase of the Reynolds number. In other words, high injection is adverse to flow reversal and prevents the effects of different expansion ratios from having a significant influence on the streamwise velocity as shown

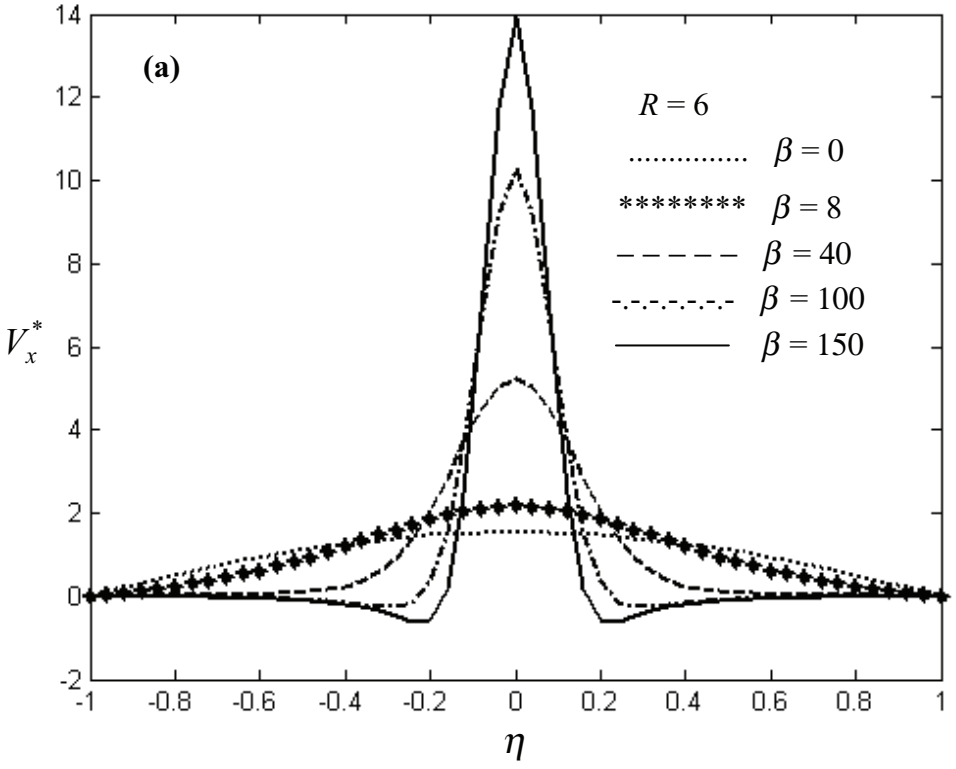

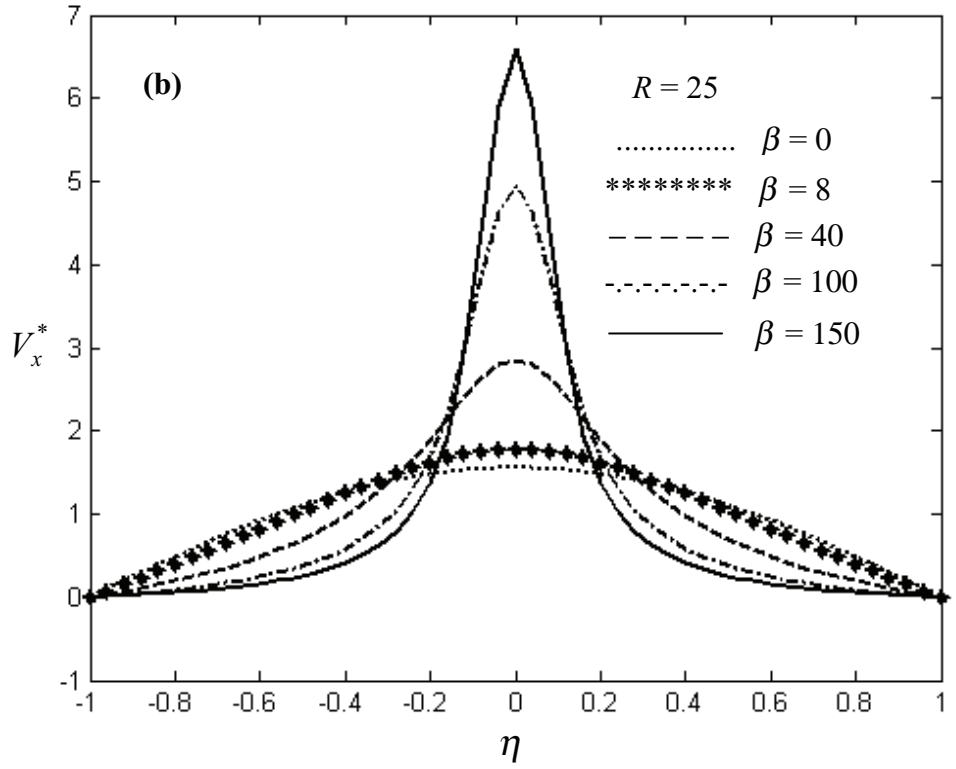

Figure 2. (Continued)

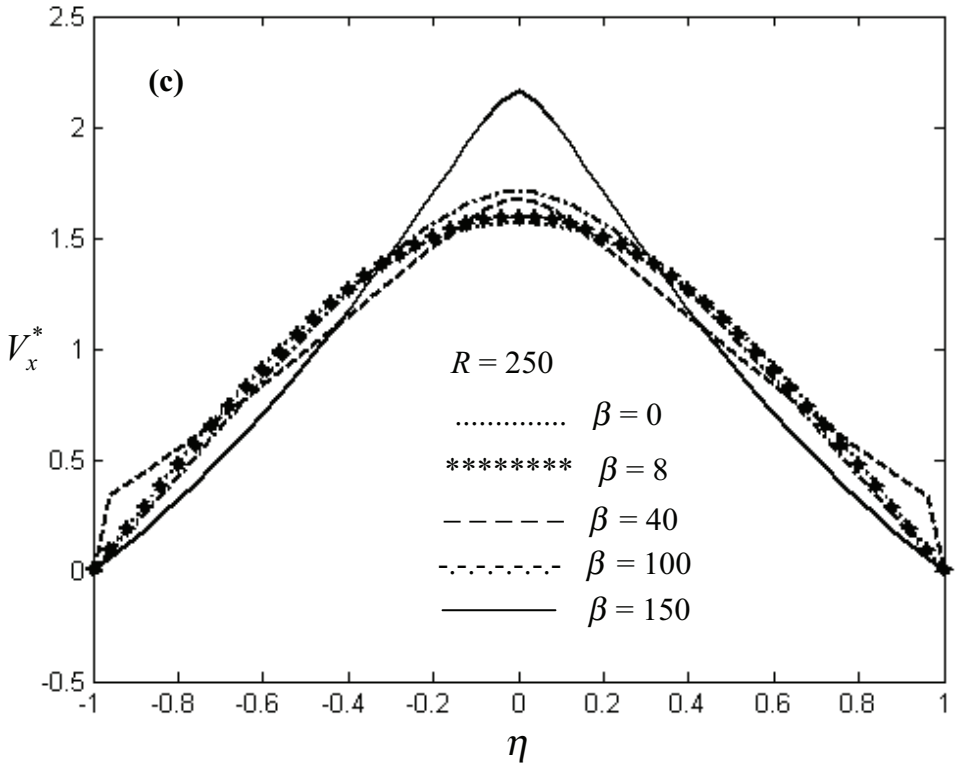

Figure 2. Streamwise velocity profiles under different expansion ratios, (a) R = 6, (b) R = 25 and (c) R = 250.

in Figure 2(c) where the computed branches of the solution tend to a same constant curve for R = 250, and for β < 100. It is also noticeable that the maximum of the stremwise velocity situated at the center of the channel as presented in Figure 2, diminishes with the increase of the Reynolds number.

The normal velocity as plotted in Figure 3(a) presents some zones around the center of the channel where it exceeds its value at walls. This is due to high expansion which gives rise to flow reversal in the case of low injection; that is the case where the collision scenario between fluid particles takes place inside the channel. It appears from Figure 3(a) that, for low Reynolds numbers, great values of the expansion ratio lead the normal velocity to exceed its value at walls because the collision increases the normal velocity of fluid particles in some zones located in the neighborhood of the middle of the channel. Furthermore, in light of Figure 3(a) and (b), the normal velocity presents different behaviors on the right and left hand sides of the center of the channel. For clarity, this normal velocity decreases with the expansion ratio on the left hand side of the middle of the flow region, while it increases on the right hand side. This behavior is due to the symmetry established at the center of the channel through the boundary conditions. The effects caused by the increase of the Reynolds number on the normal velocity distribution are similar to those mentioned about the streamwise velocity. Indeed, the normal velocity tends to a same constant curve with the growth of R under different expansion ratios as shown in Figure 3(c). At this stage, it is relevant to note that the curves plotted in Figure 3(c) for R = 250, and for various expansion ratios tend to satisfy the Taylor profile given by $V_y^* = \sin\left(\frac{1}{2}\pi\eta\right)$, as found in a previous study [23]. To summarize, the results from calculations show that, when the relative importance of the expansion ratio with respect to the Reynolds number is such as $\beta/R < 0.1$, different solution branches of the nondimensional transverse velocity V_y^* become indistinguishable from the above Taylor profile.

Since the streamwise pressure gradient per unit length is constant inside the channel, our attention is focused on the normal pressure gradient. Instead of examining pressure itself, it is convenient to describe the pressure gradient as it has a direct influence in the momentum conservation. Function $p^{(1)*}(\eta)$ plotted in Figure 4 denotes the nondimensional normal pressure gradient distribution under

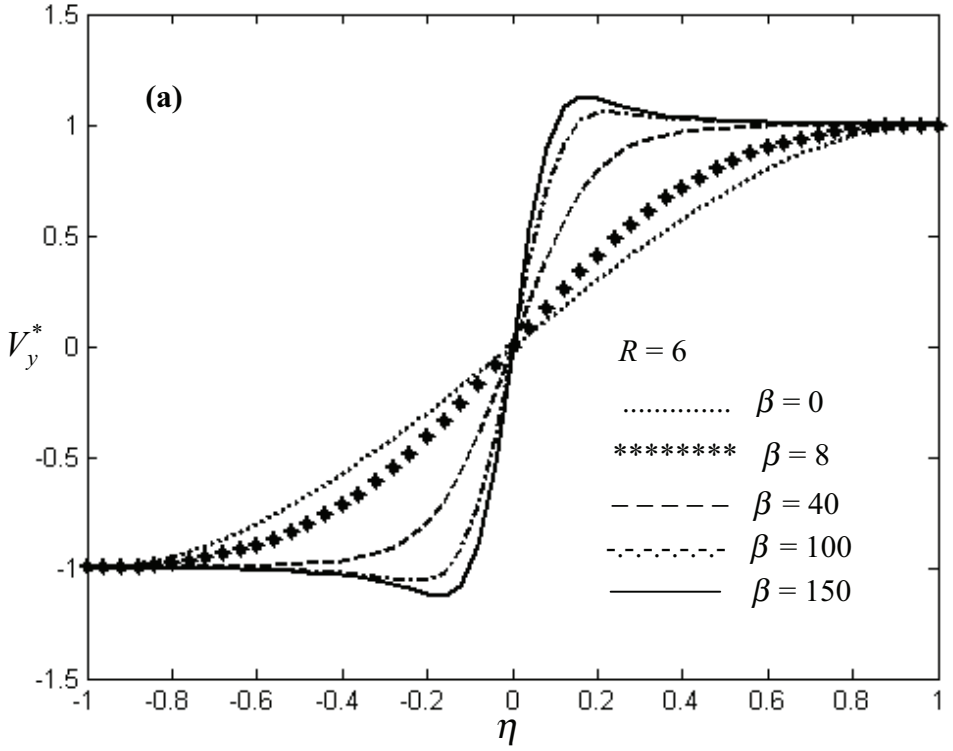

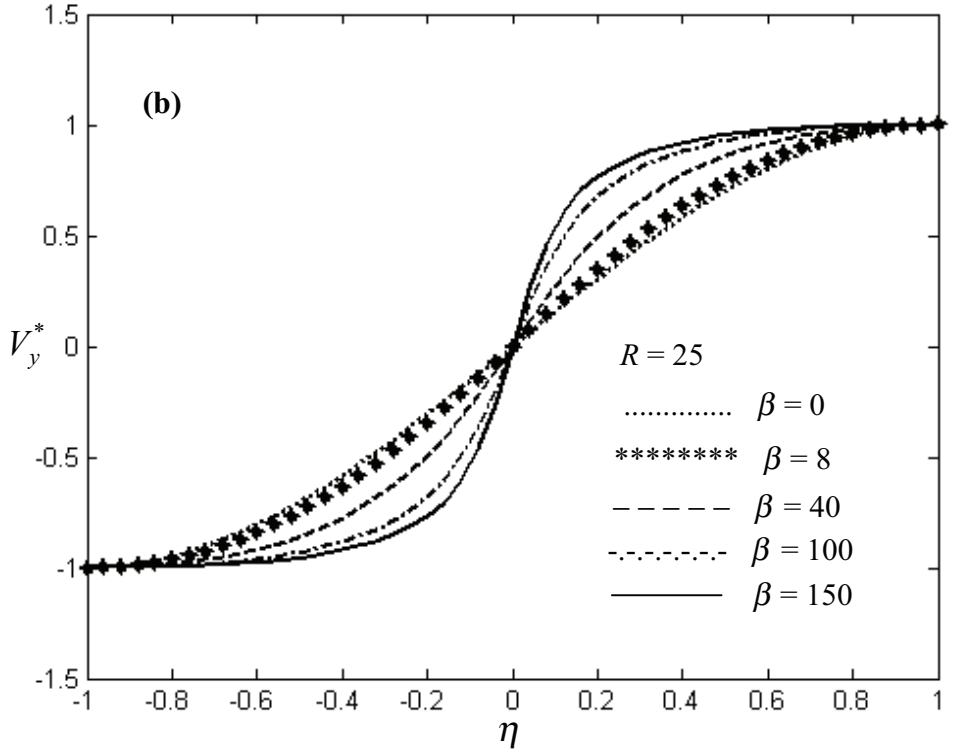

Figure 3. (Continued)

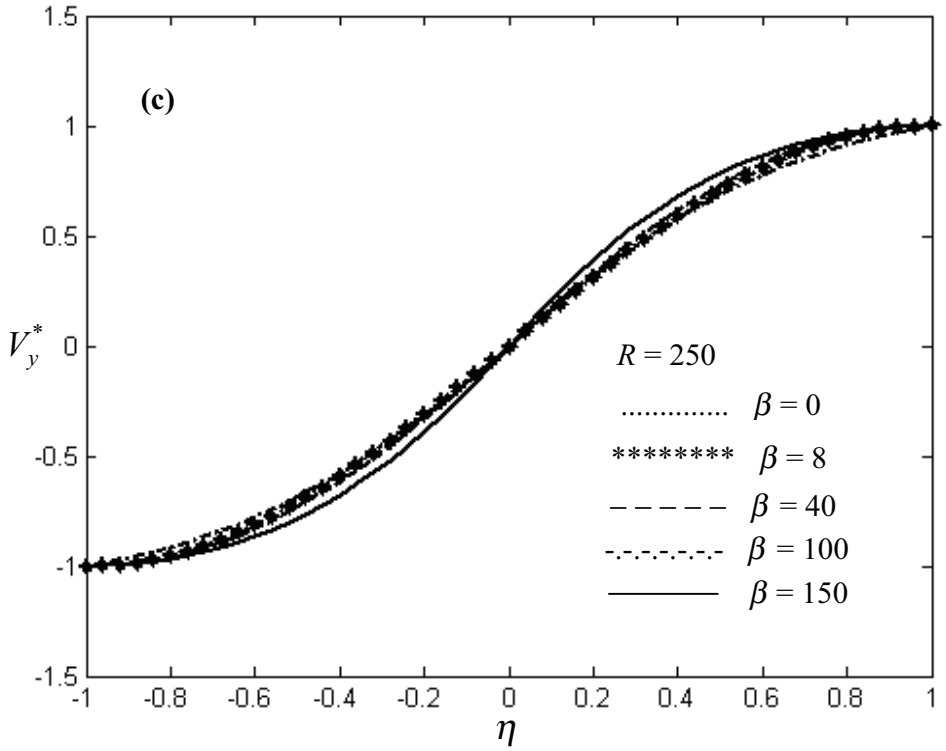

Figure 3. Normal velocity profiles under different expansion ratios, (a) R = 6, (b) R = 25 and (c) R = 250.

various values of control parameters. The curves in these figures present an inflection area around the center of the channel due to symmetry properties with respect to the midsection plane at $\eta = 0$. This inflection characterizes the fact that, normal pressure gradient increases with the expansion ratio in the region $-1 \le \eta \le 0$ and decreases in the region $0 \le \eta \le 1$. Furthermore, as the normal pressure gradient cancels at $\eta = 0$, it follows that normal pressure itself is constant at the center of the channel. This result about the normal pressure gradient which cancels at the center is in accordance with the velocity distribution. Indeed, the normal pressure is constant at the center of the channel because there is no normal motion of fluid particles by referring to the boundary conditions. On the other hand, an oscillatory pressure behavior is shown in Figure 4(c) under high injection and various expansion ratios. This means that, the inflection which occurs through the evolution of the normal pressure gradient gives rise to an oscillatory behavior with the increase of the Reynolds number.

The similarity vorticity equation is only influenced by the Reynolds number R and the expansion parameter β, while the energy equation is described by these control numbers and the Prandtl number Pr. The two ordinary differential equations of the problem are in partial coupling; more precisely, the energy equation requires solutions of the vorticity equation to be solved, but solutions from the vorticity equations are obtained without considering any parameter about the energy equation. Hence, after determining the behaviors of velocity components and pressure gradients, temperature and thermal gradients can now be presented.

In view of the boundary conditions, temperature increases inside the channel from the cold wall to the hot one and presents different concavities on the left and right hand sides of the center of the flow domain. The first concavity situated on the left hand side of the middle of the channel is turned towards the top and the second concavity located on the right hand side is turned towards the stocking as shown in Figure 5. This described behavior of temperature which is revealed identical in the problem under study for any control parameter, illustrates the presence of the inflection area around the midsection plane. The inflection through the temperature distribution is also found in a previous study [19].

The minima of thermal gradients are located near the walls, since temperature in these zones does not vary enough due to the renewal process of fluid particles by injection as shown in Figure 6. In this figure, it appears that the maximum of these thermal gradients are situated at the center of the flow region,

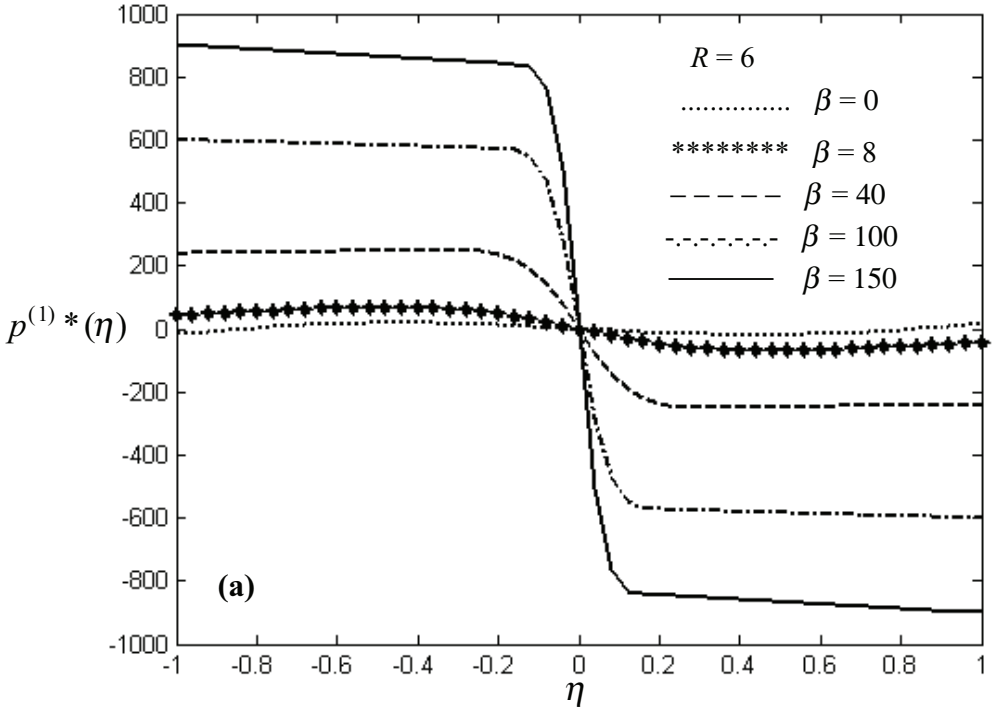

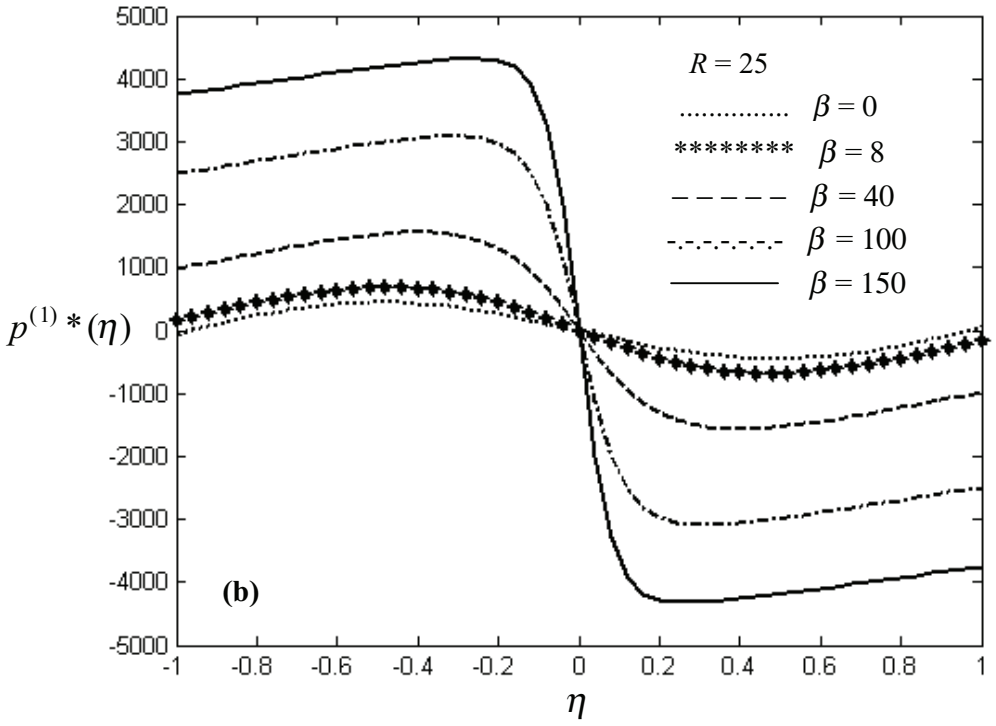

Figure 4. (Continued)

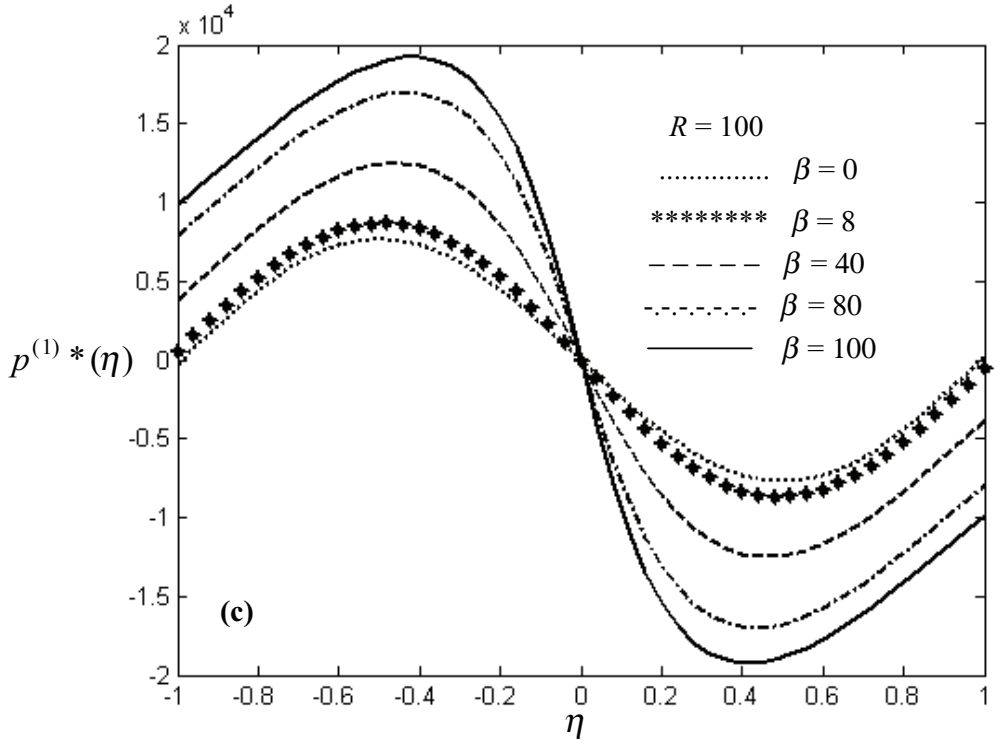

Figure 4. Normal pressure gradient under different expansion ratios, (a) R = 6, (b) R = 25 and (c) R = 100.

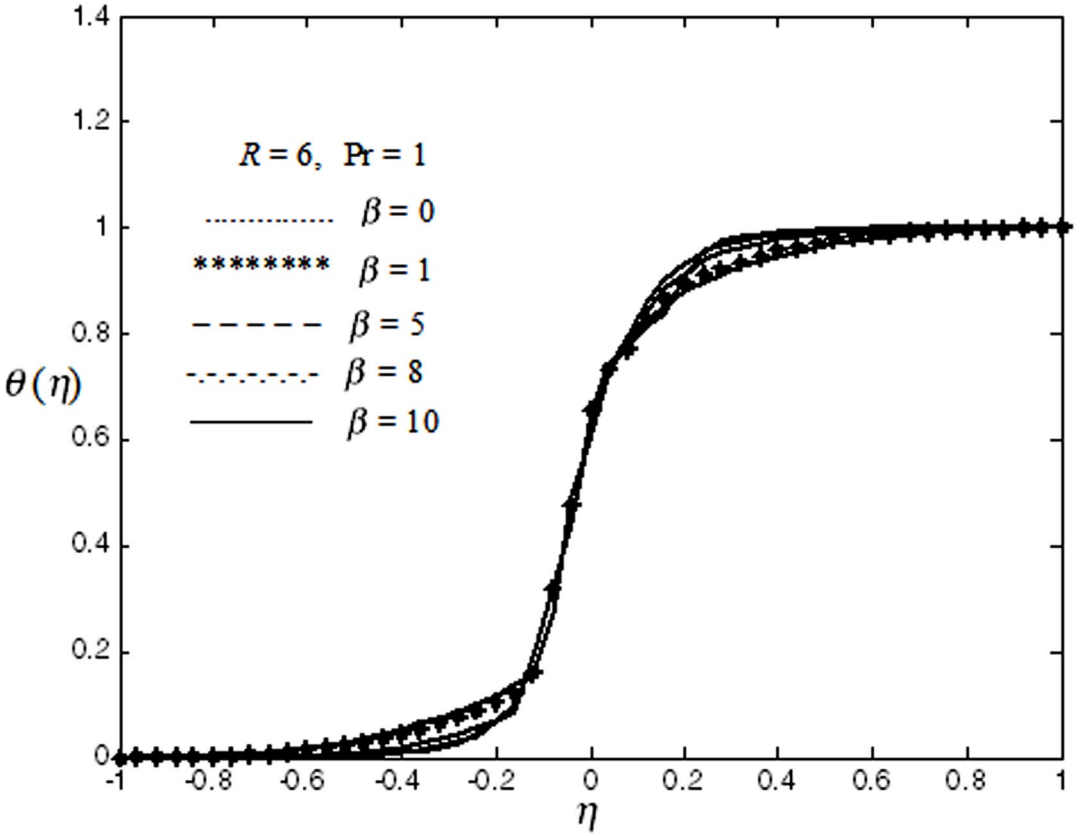

Figure 5. Temperature under different expansion ratios for R = 6 and Pr = 1.

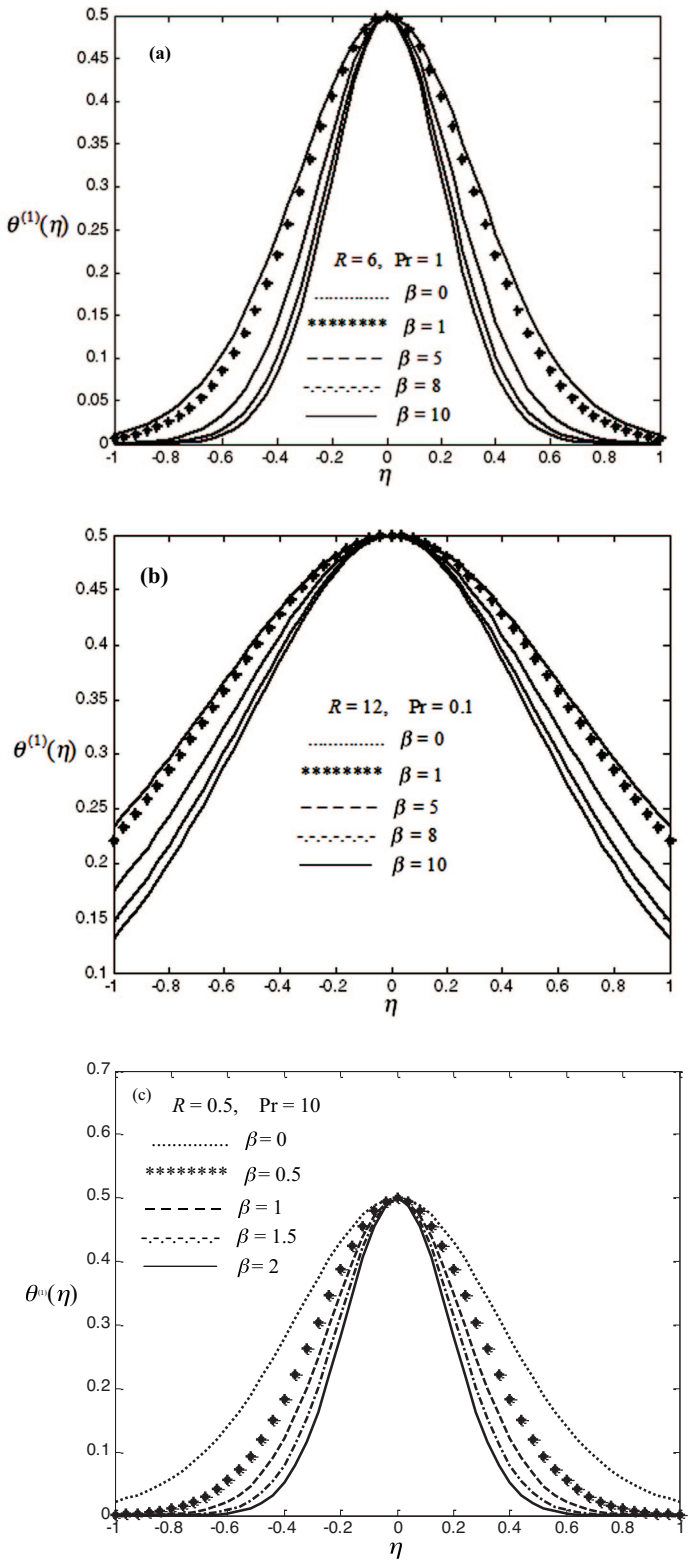

Figure 6. Thermal gradient under different expansion ratios, (a) R = 6, Pr = 1, (b) R = 12, Pr = 0.1 and (c) R = 0.5, Pr = 10.

where the temperature variations are important. It is relevant to note that, thermal behaviors presented in this study agree with those encountered in the literature. Indeed, for most studies of Berman flows with thermal influences, the channel exhibits either injection or suction across two opposing permeable walls. It is well known that, suction increases thermal gradients at walls. However, injection diminishes those thermal gradients at walls as found in the present study. The particular effect of wall expansion in this investigation is adverse to thermal gradients since Figure 6 shows that function $\theta^{(1)}(\eta)$ decreases with the parameter β under different values of the Reynolds and Prandtl numbers.

6. CONCLUSIONS

The steady flow and heat transfer across a rectangular channel with simultaneous injection and orthogonally moving walls were studied theoretically. The mathematical model of the problem was achieved using the Navier-Stokes equations and the energy equation. The flow was assumed to be two-dimensional with two non-vanished velocity components, so the stream function was introduced in the Navier-Stokes equations to obtain the vorticity transport equation. By applying the method of similarity solution, the steady problem was reduced to a set of a fourth-order and a second-order nonlinear ordinary differential equations. The solutions of the problem were found by means of a numerical scheme based on the shooting method associated with the fourth-order Runge-Kutta algorithm.

The numerical results showed that high injection is adverse to the reverse flow inside the channel. When the relative importance of the expansion ratio with respect to the Reynolds number satisfies the relationship $\beta/R < 0.1$ through the flow domain, flow reversal disappears and the normal velocity tends to a same constant curve. The increase of the Reynolds and Prandtl numbers provides oscillatory pressure gradients. The minima of thermal gradients are located at the walls due to injection.

Finally, it may be interesting to examine in future studies the spatial stability of the solutions found in this investigation.

ACKNOWLEDGEMENTS

The authors would like to thank the Reviewers for the corrections they have made and the valuable comments they have suggested for improving the paper.

NOMENCLATURE

T_{min} cold wall temperature
x streamwise coordinate
y normal coordinate
$b(t)$ channel half-spacing
h channel height
$\dot{b}$ wall moving velocity
V absolute velocity of fluid particles at walls
V_x streamwise velocity inside the channel
V_y normal velocity inside the channel
U mean flow velocity at an arbitrary location x
V_0 fluid injection velocity at walls
u_j derivative of function φ with respect to a_j
w_j derivative of function θ with respect to a_j
T_0 hot wall temperature
p pressure inside the channel
T temperature inside the channel
S cross section surface
A surface of the two horizontal walls
G_1, G_2, G_3 guess functions
F Function to minimize
n iteration index
$[J]$ Jacobian matrix
x^* nondimensional streamwise coordinate
V_x^* nondimensional streamwise velocity
V_y^* nondimensional normal velocity
p^* nondimensional pressure
$p^{(1)*}(\eta)$ nondimensional normal pressure gradient
a_1, a_2, a_3 input initial guesses
a_1^*, a_2^*, a_3^* best initial guesses

Greek Symbols

η similarity variable
ψ stream function
Φ nondimensional unsteady stream function
Θ nondimensional unsteady temperature
φ nondimensional steady stream function
θ nondimensional steady temperature
ϑ volume of the channel
ρ specific mass of the fluid
ν kinematic viscosity of the fluid
κ thermal conductivity of the fluid
β expansion ratio (wall moving ratio)

REFERENCES

[1] Da Costa, A.R., Fane, A.G. and Wiley, D.E., Spacer Characterization and Pressure Drop Modeling in Spacer-filled Channels for Ultrafiltration, *Journal of Membrane Science*, 1994, 87(1–2), pp. 79–98.

[2] Pharoah, J. G., Dijlali, N. and Vickers, G.W., Fluid Mechanics and Mass Transport in Centrifugal Membrane Separation, *Journal of Membrane Science*, 2000, 176(2), pp. 277–289.

[3] Zhou, C. and Majdalani, J., Improved Mean-flow Solution for Slab Rocket Motors with Regressing Walls, *Journal of Propulsion and Power*, 2002, 18(3), pp. 703–711.

[4] Jones, R.T., Blood Flow, *Annual Review of Fluid Mechanics*, 1969, 1(1), pp. 223–244.

[5] Sorour, M.M. and Hassab, M.A., Effect of Sucking the Hot Fluid Film on the Performance of Flat Plate Solar Energy Collectors, *Applied Energy*, 1983, 14(3), pp. 161–173.

[6] Raithby, G., Laminar Heat Transfer in the Thermal Entrance Region of Circular Tubes and Two-dimensional Rectangular Ducts with Wall Suction and Injection, *International Journal of Heat and Mass Transfer*, 1971, 14(2), pp. 223–243.

[7] Raithby, G.D. and Knudsen, D.C., Hydrodynamic Development in a Duct with Suction and Blowing, *Journal of Applied Mechanics*, 1974, 41, pp. 896–902.

[8] Rhee, S.J. and Edwards, D.K., Laminar Entrance Flow in a Flat Plate Duct with Asymmetric Suction and Heating, *Numerical Heat Transfer*, 1981, 4(1), pp. 85–100.

[9] Robinson, W.A., The Existence of Multiple Solutions for the Laminar Flow in a Uniformly Porous Channel with Suction at Both Walls, *Journal of Engineering Mathematics*, 1976, 10(1), pp. 23–40.

[10] Berman, A.S., Laminar Flow in Channels with Porous Walls, *Journal of Applied Physics*, 1953, 24(9), pp. 1232–1235.

[11] Martins-Costa, M.L., Saldanha da Gama, R.M. and Frey, S., Modeling of a Generalized Newtonian Flow through Channels with Permeable Wall, *Mechanics Research Communications*, 2000, 27(6), pp. 707–712.

[12] Majdalani, J. and Zhou, C., Moderate-to-large Injection and Suction Driven Channel Flows with Expanding and Contracting Walls, *ZAMM*, 2003, 83(3), pp. 181–196.

[13] Asghar, S., Mushtaq, M. and Hayat, T., Flow in a Slowly Deforming Channel with Weak Permeability: an Analytical Approach, *Nonlinear Analysis* : *Real World Applications*, 2010, 11(1), pp. 555–561.

[14] Li, B., Zheng, L., Zhang, X. and Ma, L., The Multiple Solutions of Laminar Flow in a Uniformly Porous Channel with Suction/Injection, *Advance Studies in Theoretical Physics*, 2008, 2(10), 473–478.

[15] Ge, M.-W., Xu, C.-X. and Cui, G.-X., Study on Flow Structures due to a Dimple in Channel Flow by Direct Numerical Simulation, *International Journal of Flow Control*, 2012, 4(1–2), pp. 67–82.

[16] Brady, J.F., Flow Development in a Porous Channel or Tube, *Physics of Fluids*, 1984, 27(5), pp. 1061–1067.

[17] Banks, W.H.H. and Zaturska, M.B., On Flow through a Porous Annular Pipe, *Physics of Fluids A*, 1992, 4(6), pp. 1131–1141.

[18] Majdalani, J. and Flandro, G.A., The Oscillatory Pipe Flow with Arbitrary Wall Injection, *Proceedings of the Royal Society of London A*, 2002, 458(2023), pp. 1621–1651.

[19] Hona, J., Ngo Nyobe, E. and Pemha, E., Dynamic Behavior of a Steady Flow in an Annular Tube with Porous Walls at Different Temperatures, *International Journal of Bifurcation and Chaos in Applied Science and Engineering*, 2009, 19(9), pp. 2939–2951.

[20] Massoudi, M., Flow of a Binary Mixture of Linearly Incompressible Viscous Fluids Between Two Horizontal Parallel Plates, *Mechanics Research Communications*, 2008, 35(8), pp. 603–608.

[21] Ferro, S. and Gnavi, G., Effect of Temperature Dependent Viscosity in Channels with Porous Walls, *Physics of Fluids*, 2002, 14(2), pp. 839–849.

[22] Brady, J.F. and Acrivos, A., Steady Flow in a Channel or Tube with an Accelerating Surface Velocity. An Exact Solution to the Navier–Stokes Equations with Reverse Flow, *Journal of Fluid Mechanics*, 1981, 112, pp. 127–150.

[23] Taylor, G.I., Fluid Flow in Regions Bounded by Porous Surfaces, *Proceedings of the Royal Society of London*, 1956, 234(1199), pp. 456–475.